Multi-channel laser interferometer based on automatic frequency stabilization system for improving coordinate measurement accuracy*

PANG Chengkai[1,2], ZHANG Qiongqiong[1], ZHANG Hongqiao[1], HUANG Haiyan[1], DENG Zejiang[1], and WU Guang[1,3]**

1. State Key Laboratory of Precision Spectroscopy, East China Normal University, Shanghai 200241, China

2. Chongqing Key Laboratory of Precision Optics, Chongqing Institute of East China Normal University, Chongqing 401120, China

3. Collaborative Innovation Center of Extreme Optics, Shanxi University, Taiyuan 030006, China

(Received 15 April 2022; Revised 29 May 2022)

A multi-channel laser interferometer (MCLI) is proposed to improve the coordinate measurement accuracy. A 780 nm external cavity laser is locked on the D_2 line of ^{87}Rb atom by polarization spectroscopy, and a high frequency stabilized laser source is obtained with a linewidth of 385.8 kHz at root mean square (*RMS*). The interferometers share the stabilized source and individually install on 4 axes of a coordinate measuring system. As a result, the measurement uncertainty is reduced from 1.2 μm to 0.2 μm within the dynamic measurement range of 1.0 m. The MCLI is adept at integrate and flexible installation, which caters to various applications on precision measurement.

Document code: A **Article ID:** 1673-1905(2022)10-0588-7

DOI https://doi.org/10.1007/s11801-022-2063-0

Laser precision measurement technology plays an important role in aerospace, automobile manufacture, semiconductor manufacturing and other fields for the advantages of high precision and high efficiency[1-6], such as the inspection of aeroengine blades, the measurement and location of integrated chips in lithography. Coordinate measuring machines (CMMs) have stronger advantages over other measurement devices, particularly for versatility and high precision, which are widely used in the micron level measurement[7-15]. CMMs combine the coordinate information provided by the grating rulers and the range information provided by the measuring head to realize profile measurement of large targets[16]. However, with the increase of the movement distance, the error introduced by the grating rulers increases gradually, resulting in the decrease of the measurement accuracy[17,18]. Therefore, it is vital to improve the coordinate measurement accuracy of CMMs when the high-precision large profile measurement is achieved. Laser interferometer has the ability of large-range and high-precision displacement measurement[19-24], becoming a highly competitive technology of coordinate measurement. And a few leading technology companies in the field of measurement began to try this application, such as Renishaw and Attocube. Conventional laser interferometer consists of three independent modules, including laser and detector, beam splitting and combining, and reflectors, to form the optical path of laser interferometry. Commonly it is bulky, expensive, and complex to install the laser interferometer on CMMs.

In this paper, a multi-channel laser interferometer (MCLI) for the coordinate measurement of CMMs is proposed. The optical interference path is simplified as two independent modules, which can be easily installed on the CMM. This split structure design improves the integration of laser interferometer and makes its application more valuable in industry, which has been well popularized in commercial market, such as SIOS SP 2000. The laser source with frequency stabilized is helpful to improve the accuracy of interferometry. Polarization spectroscopy is widely applied to the laser frequency locking technique which does not require external frequency modulation and can achieve high frequency stability[25,26]. In this work, the automatic frequency stabilization is realized on a field programmable gate array (FPGA) board, which simplifies the process and improves the efficiency of frequency stabilization. A 780 nm external cavity laser is locked on the ^{87}Rb D_2 line with the help of polarization spectroscopy, and the output laser is distributed to each multiple interferometer through optical fiber. The coordinate measurement uncertainty of a single axis of the CMM is reduced from

* This work has been supported by the National Natural Science Foundation of China (Nos.11774095, 11804099, and 11621404), and the Research Funds of Happiness Flower ECNU (No.2021ST2110).

** E-mail: gwu@phy.ecnu.edu.cn

1.2 μm to 0.2 μm in the range of 1.0 m. It provides an economical and robust approach to improve the coordinate measurement precision.

In the single frequency laser interferometry displacement measurement, a frequency stabilized laser source is divided into reference part and signal part. The reference and signal beams satisfy

$$\begin{cases} E_R(t) = A_R \cdot \cos(\omega t + \Phi_R) \\ E_S(t) = A_S \cdot \cos(\omega t + \Phi_S) \end{cases}, \tag{1}$$

where $E_R(t)$ and $E_S(t)$ are electric fields of reference light and signal light, respectively. A_R and A_S represent their amplitudes, and $\omega t+\Phi_R$ and $\omega t+\Phi_S$ are the phases of the two lasers at the time t. In the experiment, $A_R=A_S=A$. When two beams of light interfere with each other and enter the detector, the voltage on the load resistance R_L is

$$\begin{cases} V = SR_L[A^2\cos(\Delta\Phi) + A^2] \\ \Delta\Phi = \Phi_R - \Phi_S \end{cases}, \tag{2}$$

where S is photon sensitivity of the optical detector, and $\Delta\Phi$ is the phase difference between the reference light and the signal light. In the process of target movement, the real-time voltage change collected by the photodetector can be converted into the phase change, which realizes nanometer displacement measurement in a large range. The integral part of the voltage period is recorded as m, and the fractional part as n. The displacement is calculated by

$$L = \frac{\lambda}{2}\cdot(m+n). \tag{3}$$

In order to determine the direction of movement, each interferometer has two sub-interferometers, interferometer 1 and interferometer 2. As shown in Fig.1(a), two laser beams with the same wavelength and phase (indicated by red and blue) are divided into two reference beams and two signal beams through beam splitter (BS). After passing through the phase modulation module, π/2 phase difference between the two reference beams is generated. The phases of two signal beams are the same. Hence the interference signals between interferometer 1 (CH1) and interferometer 2 (CH2) will produce a phase difference of π/2. The interference signals can be expressed as

$$\begin{cases} V_1 = SR_L[A^2\cos(\Delta\Phi_1) + A^2] \\ \Delta\Phi_1 = \Phi_{R2} - \Phi_S \\ V_2 = SR_L[A^2\cos(\Delta\Phi_2) + A^2] \\ \Delta\Phi_2 = \Phi_{R2} - \Phi_S \end{cases}, \tag{4}$$

where V_1 and V_2 are the output voltages, and $\Delta\Phi_1$ and $\Delta\Phi_2$ are the phase differences of two sub-interferometers, respectively. The interferogram of a target in uniform motion is shown in Fig.1(b). The direction of movement cannot be determined by only interferometer 1, while $\Delta\Phi_1 \approx k\pi$ (k=0, 1, 2, 3…). So, interferometer 2 is added. $\Delta\Phi_1-\Delta\Phi_2\approx\pi/2$. For an example, in the blue dotted box, V_2 decreases while the target moves in the positive direction, and rises in the opposite direction. Therefore, the combination of two sub-interferometers realizes tracking measurement.

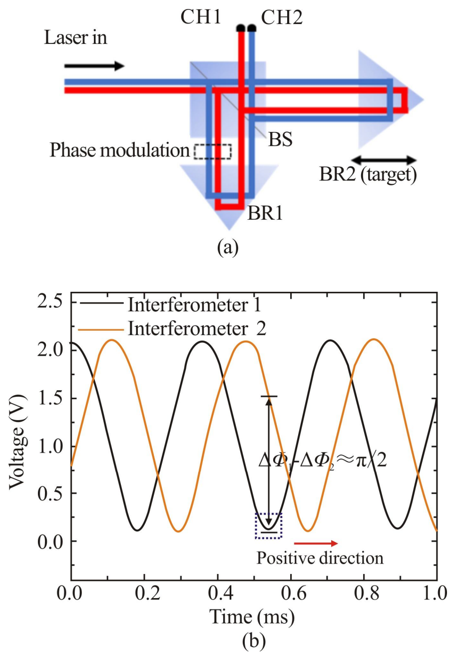

BS: beam splitter; BR: backward reflector; CH: channel of interferometer

Fig.1 (a) Schematic diagram of interferometer; (b) Interferogram of the target in uniform motion

The flow chart of interferometer data processing is shown in Fig.2(a), where L, L', and N are the displacement, displacement register value, and the count of half interference period. First, 10^6 sampling points of each interferometer are packaged into a group and normalized. As shown in Fig.2(b), the two data groups have several intersections, and the sampling points between two intersections are treated as one data segment. The displacement between the first and last intersection L_{seg} can be expressed as

$$L_{seg} = \frac{\lambda}{4}\cdot N. \tag{5}$$

The displacement of the target before the first intersection is recorded as L_{start}, and that after the last intersection as L_{stop}. $\Delta\varphi_{start1}$ and $\Delta\varphi_{start2}$ are the phase differences of interferometer 1 and interferometer 2 before the first intersection, respectively. $\Delta\varphi_{stop1}$ and $\Delta\varphi_{stop2}$ are the phase differences of interferometer 1 and interferometer 2 after the last intersection, respectively. When processing the first data group, L_{start} and L_{stop} can be expressed as

$$L_{start} = \frac{\lambda}{2}\cdot\frac{\arccos\Delta\varphi_{start1} + \arccos\Delta\varphi_{start2}}{2}, \tag{6}$$

$$L_{stop} = \frac{\lambda}{2}\cdot\frac{\arccos\Delta\varphi_{stop1} + \arccos\Delta\varphi_{stop2}}{2}. \tag{7}$$

The next step is to determine the moving direction of the target. It is specified as the positive direction of target movement when the phase of interferometer 1 is in front of interferometer 2. When the target moves in the positive direction, the count N count plus 1, otherwise N minus 1. N remains unchanged when the target jitters. Repeat this step if there are unprocessed data segments. At last, the value of L is output, if there is no remaining data group.

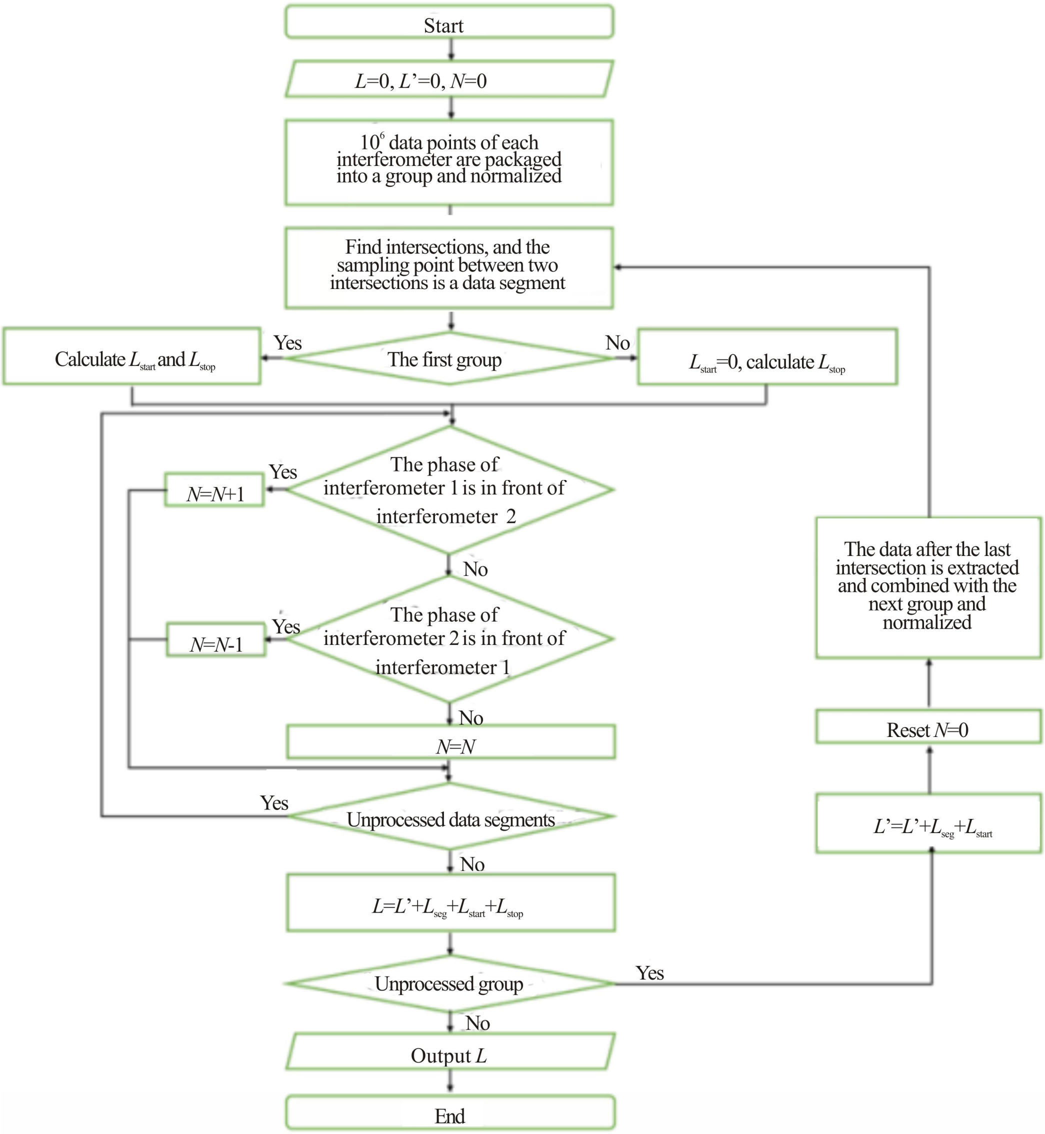

(a)

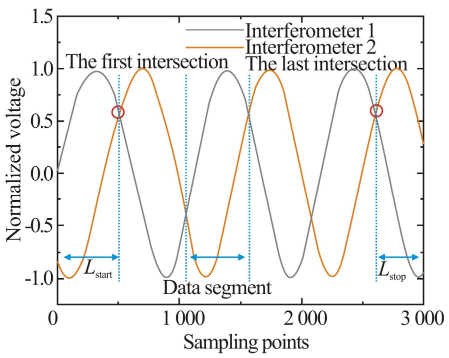

(b)

Fig.2 (a) Flow chart of interferometer data processing; (b) Normalized interferogram

The experimental setup is shown in Fig.3. Fig.3(a) is the frequency stabilization system of the laser. The linearly polarized light emitted from the semiconductor laser is divided into two beams by a beam splitter (BS1) after passing through an optical isolator (OI). One beam is coupled into a polarization maintaining fiber (PMF) coupler and distributed to each laser interferometers. To fulfill the frequency stabilization, the other beam is divided and performs as strong pump light and weak probe light after being manipulated by a half-wave plate (HWP) and a polarization beam splitter (PBS). The pump light is converted into circularly polarized light by a quarter-wave plate (QWP). The strong circularly polarized pump light and the weak linearly polarized probe light are superimposed in an Rb atomic vapor cell in reverse. In the absence of circularly polarized pump light, Rb atoms are approximately uniformly distributed in Zeeman states with different ground states. Due to the different Clebsch-Gordan (CG) coefficients between different Zeeman states, the atomic populations in different Zeeman states are asymmetric when the circularly polarized pump light passes through the Rb atomic vapor cell, which causes the anisotropy of atomic medium and shows different absorptions of left and right circularly polarized light for atoms in different Zeeman states. The linearly polarized probe light can be regarded as the superposition of left and right circularly polarized light according to the specific phase difference. The left and the right circularly polarized light beams have different absorptions of atoms and different propagation velocities in the Rb atomic vapor cell, which leads to the change of the phase difference of these two circularly polarized light beams, and finally the polarization of the probe light is changed. After sequentially passing through the Rb atomic vapor cell, HWP and PBS, the linearly polarized probe light is captured by a differential balance detector (DBD). The triangular waveform is superimposed on the feedback terminal of the laser to obtain the polarization spectroscopy, which is used as the frequency discrimination curve. The laser wavelength is locked on the ^{87}Rb D_2 line at 780.246 nm. Fig.3(b) is the multi-channel laser interferometry displacement measurement system. The laser is coupled into the PMF coupler, and emitted a collimated laser beam of 4 mm in diameter. The light is divided into reference light and signal light by BS3. The casting angle of the signal light is adjusted by a mirror (M3) to make the optical axis parallel to the target movement direction. A piece of polished optical glass is inserted between BS3 and the backward reflector (BR1) to half shadow the reference beam and introduce a phase difference of ~π/2. The reference light interferes with the reflected signal light and then incident on two silicon photomultipliers (Si-PMs). The two Si-PMs are operated in linear mode, and generate two orthogonal phase signals, which are collected by data acquisition (DAQ) card (NI USB-6356) and processed by a computer to calculate displacement information.

Fig.4(a) is the picture of the frequency stabilization system. As shown in Fig.4(b), two PIN photodiodes (Hamamatsu, S12271) with large sensitive area of 4.1 mm in diameter are used to constitute the DBD. The size of the laser interferometer is shown in Fig.4(c). Fig.4(d) is the internal setup of the interferometer. Fig.4(e) shows the combination of the MCLI and the CMM. The frequency stabilized light source was distributed to 4 interferometers installed on the *X*-axis, *Y*-axis, *Y*-axis slave arm and *Z*-axis of the CMM through PMF coupler.

The measurement accuracy of laser interferometer is affected by the stability of laser frequency, and the uncertainty can be expressed as

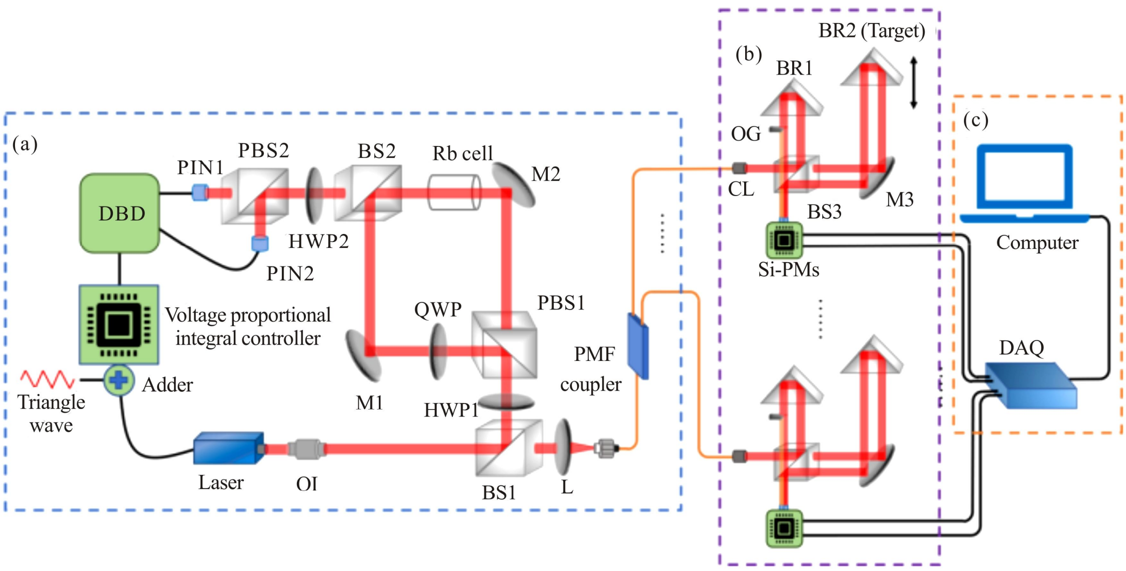

OI: optical isolator; BS: beam splitter; PBS: polarized beam splitter; HWP: half-wave plate; QWP: quarter-wave plate; M: mirror; L: lens; DBD: differential balance detector; PMF: polarization maintaining fiber; CL: collimator; BR: backward reflector; OG: optical glass; Si-PM: silicon photomultiplier; DAQ: data acquisition card

Fig.3 Experimental setup with (a) laser frequency stabilization system, (b) multi-channel laser interferometry ranging system, and (c) DAQ and processing system

$$\begin{cases} \Delta\lambda = \dfrac{\Delta\nu \cdot \lambda^2}{c} \\ \Delta L = \dfrac{2L}{\lambda} \cdot \Delta\lambda \end{cases}, \tag{8}$$

where L is the measurement displacement. Therefore, the more stable the laser frequency, the higher the measurement accuracy of the interferometer. In the laser frequency stability test, a DAQ card was used to collect the voltage data. The automatic frequency stabilization is realized on a FPGA board, and the schematic is shown in Fig.5(a). The triangular wave generated by the FPGA is loaded on the scanning port of laser driver, and the bias voltage of triangular wave is gradually increased. The bias voltage is stopped increasing and the triangular wave is removed, when the frequency discrimination curve obtained by the DBD is consistent with the standard frequency discrimination curve. The frequency of the laser is near the target frequency. Then the generated signal of the proportional integral (PI) circuit is loaded into the feedback port on the laser driver to achieve the frequency stabilization. The frequency discrimination curve is shown in Fig.5(b). The PI control circuit was used to lock the laser at the absorption peak in the black frame, and the wavelength was locked on the ^{87}Rb D_2 line at 780.246 nm. The frequency jitter of the stabilized laser is shown in Fig.5(c). The standard deviation of laser frequency jitter Δv stayed at 385.8 kHz during 40 min.

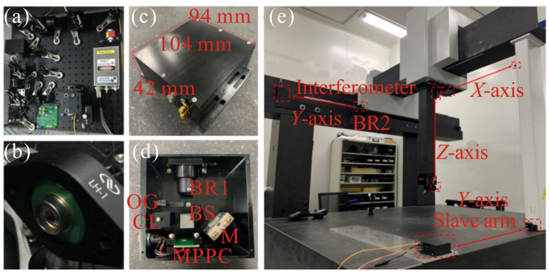

Fig.4 (a) Photograph of the frequency stabilization system; (b) DBD consisting of two PIN photodiodes; (c) Size of interferometer; (d) Internal setup of interferometer; (e) MCLIs installed in CMM

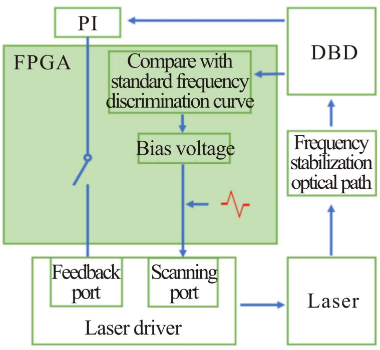

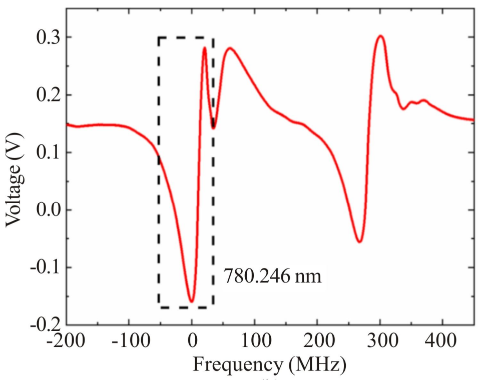

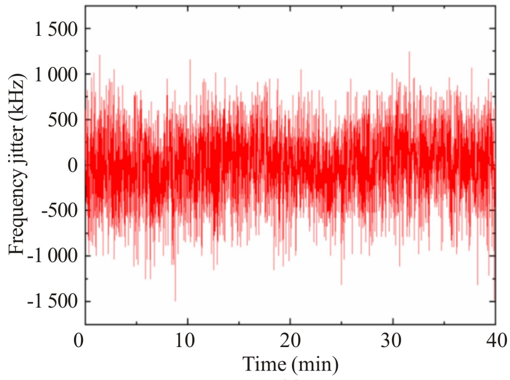

Fig.5 Frequency stability analysis: (a) Schematic of automatic frequency stabilization; (b) Frequency discrimination curve; (c) Frequency jitter curve

The air refractive index is sensitive to environmental temperature, which makes the optical path elastic and reduces the stability of the interferometer. In the interferometer stability test, the marble column of the CMM performed as the target, and the distance between the interferometer and the marble column was about 100 mm. The stability of MCLI and commercial interferometer (CHOTEST, SJ6000) was simultaneously monitored for 30 min. The environmental temperature was monitored. As shown as the grey curve in Fig.6(a), the temperature change of ~0.1 °C was recorded in 30 min. According to Edlén formula[27,28], the length change is about 10 nm for a 100 mm optical path. The displacement jitters of MCLI and commercial interferometer are shown as 17 nm and 23 nm in the orange and blue curves in Fig.6(a), respectively. The MCLI possessed a superior stability compared with the commercial interferometer. Actually, the stability of the interferometer also depends on environmental vibration, humidity and other factors, resulting in the displacement jitter greater than 10 nm. On the other hand, the *Y*-axis slave arm change of the CMM was monitored by the MCLI and the commercial interferometer for 30 min simultaneously. The displacement jitter of *Y*-axis slave arm was recorded as shown in Fig.6(b). The measurement results of the two interferometers were consistent, while the CMM remained stationary when powered on. It shows that the *Y*-axis slave arm still had a displacement jitter, and the MCLI can correctly measure these small fluctuations. Therefore, the coordinate measurement accuracy can be improved by replacing the coordinate information of grating rulers of the CMM with that measured by the MCLI.

The measurement uncertainty of the MCLI and the grating ruler of CMM was tested by comparing with the reference value offered by the commercial interferometer, and the results are shown in Fig.7. In experiment, 10^6 sampling points of each interferometer were packaged into a group, and the sampling rate of DAQ was 1 MHz. The residuals of the MCLI with different displacements are shown in Fig.7(a), and each displacement was measured 10 times. In the range of 1.0 m, the residuals increased with the increase of the displacement, which was 5×10^{-7} in relative. Fig.7(b) and (c) show the residual distributions of 105 times of measurements by the MCLI and the CMM under 1.0 m displacement. The measurement uncertainty of MCLI and CMM was 197 nm and 1.2 μm, respectively. The full width at half maximum (*FWHM*) of the residual distribution of MCLI was obviously smaller than that of CMM. The test process was carried out in a constant temperature environment of 22 °C, and the measurement uncertainty could be contributed to ambient temperature drift, air pressure fluctuation and mechanical vibration. Therefore, the coordinate measurement accuracy can be significantly improved by using the coordinate information measured by the MCLI.

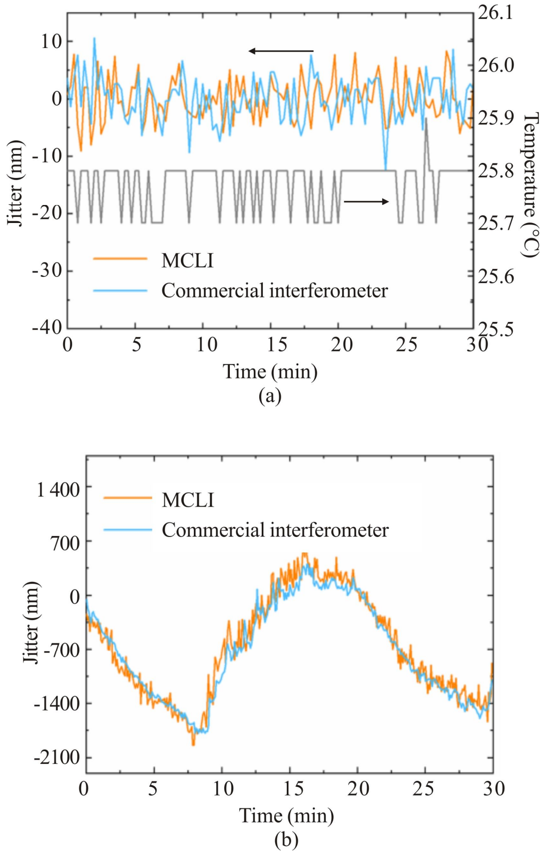

Fig.6 Displacement jitter test for (a) interferometers and (b) *Y*-axis slave arm of CMM

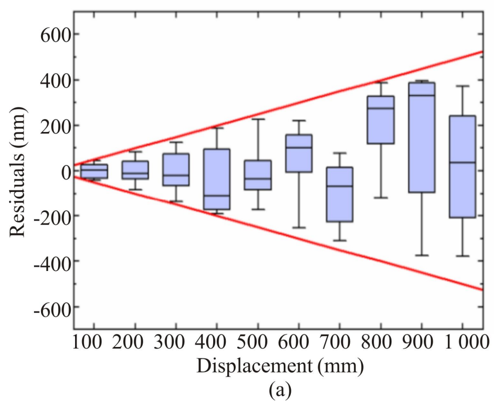

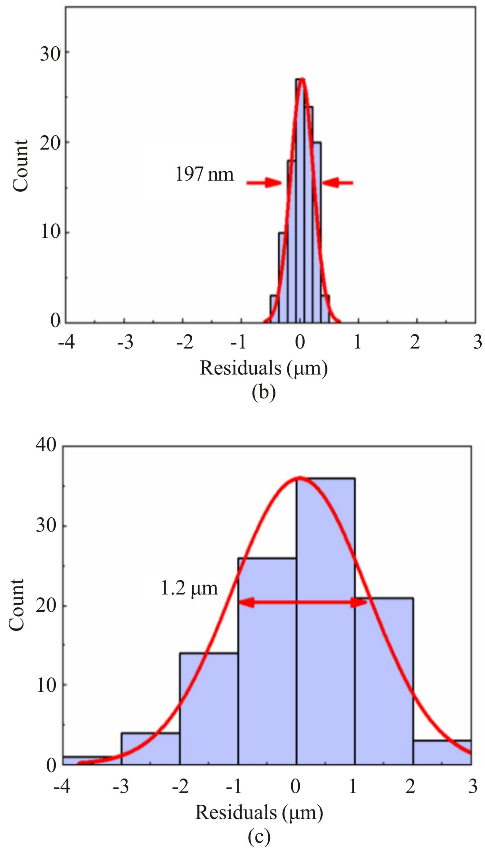

Fig.7 Residuals distributions: (a) Residuals of MCLI with different displacements; (b) Residual distribution of 105 measurements by MCLI; (c) Residual distribution of 105 measurements by CMM

In this paper, a multi-channel laser interferometer was proposed for improving coordinate measurement accuracy of the CMM. The external cavity laser was locked at 780.264 nm by polarization spectroscopy and the linewidth was 385.8 kHz at root mean square (*RMS*). The frequency stabilized laser source was delivered to the four interferometers installed on the *X*-axis, *Y*-axis, *Y*-axis slave arm and *Z*-axis of the CMM, and the coordinate measurement uncertainty of single axis of the CMM was reduced from 1.2 μm to 0.2 μm. In addition, the profile scanning demonstration of aircraft engine blade model was carried out combined with MCLI and triangular rangefinder. This technique has great potential in the application of precision manufacturing. In the succeeding work, the environmental monitoring correction module can be added by testing MCLI at different temperatures, which will improve the performance of the MCLI to realize high-precision measurement in changing environment.

Statements and Declarations

The authors declare that there are no conflicts of interest related to this article.

References

[1] HUANG J, WANG Z, GAO J, et al. Overview on the profile measurement of turbine blade and its development[J]. Proceedings of the International Society for Optical Engineering, 2010, 7656：76560L.

[2] KAWALEC A, MAGDZIAK M. The selection of radius correction method in the case of coordinate measurements applicable for turbine blades[J]. Precision engineering, 2017, 49：243-252.

[3] KANG J, WU B, SUN Z, et al. Calibration method of a laser beam based on discrete point interpolation for 3D precision measurement[J]. Optics express, 2020, 28(19)：27588-27599.

[4] KANG J, WU B, XUE T. Articulated laser sensor for three-dimensional precision measurement[J]. IEEE access, 2017, 7：121255-121264.

[5] DONG Z, SUN X, CHEN C, et al. An on-machine precision measurement method for API threads[J]. Measurement science and technology, 2019, 30：085006.

[6] LI M, ZHANG X, ZHANG J, et al. Long-range and high-precision fault measurement based on hybrid integrated chaotic laser[J]. IEEE photonics technology letters, 2019, 31(16)：1389-1392.

[7] SONG L, SUN S, YANG Y, et al. A multi-view stereo measurement system based on a laser scanner for fine workpieces[J]. Sensors, 2019, 19(2)：381.

[8] MUTILBA U, GOMEZ-ACEDO E, KORTABERRIA G, et al. Traceability of on-machine tool measurement：a review[J]. Sensors, 2017, 17(7)：1605.

[9] WANG J, CHEN P, DENG Y, et al. New algorithms for motion error detection of numerical control machine tool by laser tracking measurement on the basis of GPS principle[J]. Review of scientific instruments, 2018, 89：015104.

[10] LI Y, ZHAO Y, WANG Z, et al. Precision measurement method of laser beams based on coordinate measuring machine[J]. IEEE access, 2019, 7：112736-112741.

[11] WANG Z, ZHANG X, SHEN Y, et al. Pose calibration of line structured light probe based on ball bar target in cylindrical coordinate measuring machines[J]. Measurement, 2021, 171：108760.

[12] OSTROWSKA K, GĄSKA A, KUPIEC R, et al. Comparison of accuracy of virtual articulated arm coordinate measuring machine based on different metrological models[J]. Measurement, 2018, 133：262-270.

[13] LOU S, BROWN S, SUN W, et al. An investigation of the mechanical filtering effect of tactile CMM in the measurement of additively manufactured parts[J]. Measurement, 2019, 144：173-182.

[14] CHEN W, CHEN S, ZHAI D. Coordinate stitching measurement of highly steep freeform surfaces[J]. Measurement science and technology, 2021, 32：025009.

[15] SHEN Y, ZHANG X, WANG Z, et al. A robust and efficient calibration method for spot laser probe on CMM[J]. Measurement, 2020, 154：107523.

[16] BI C, FANG J, LI K, et al. Extrinsic calibration of a laser displacement sensor in a non-contact coordinate measuring machine[J], Chinese journal of aeronautics, 2017, 30(4)：1528-1537.

[17] WEI C, YAN S, LIN C, et al. Compact grating displacement measurement system with a 3×3 coupler[J]. Chinese optics letters, 2015, 13(5)：051301.

[18] HSU C, CHEN H, TSENG H, et al. High displacement resolution encoder by using triple grating combination interferometer[J]. Optics and laser technology, 2018, 105：221-228.

[19] WANG X, WANG X, LU H, et al. Laser diode interferometer used for measuring displacements in large range with a nanometer accuracy[J]. Optics and laser technology, 2001, 33(4)：219-223.

[20] ZHANG M, NI C, ZHU Y, et al. Sinusoidal phase-modulating laser diode interferometer for wide range displacement measurement[J]. Applied optics, 2017, 56(20)：5685-5691.

[21] JOO K, ELLIS J, BUICE E, et al. High resolution heterodyne interferometer without detectable periodic nonlinearity[J]. Optics express, 2010, 18(2)：1159-1165.

[22] WANG G, JANG Y, HYUN S, et al. Absolute positioning by multi-wavelength interferometry referenced to the frequency comb of a femtosecond laser[J]. Optics express, 2015, 23(7)：9121-9129.

[23] BERG S, PERSIJN S, KOK G, et al. Many-wavelength interferometry with thousands of lasers for absolute distance measurement[J]. Physical review letters, 2012, 108(18)：183901.

[24] KAZIEVA T, GUBSKIY K, KUZNETSOV A, et al. 3D push-pull heterodyne interferometer for SPM metrology[J]. Applied optics, 2019, 58(15)：4000-4006.

[25] PEARMAN C, ADAMS C, COX S, et al. Polarization spectroscopy of a closed atomic transition：applications to laser frequency locking[J]. Journal of physics B：atomic, molecular and optical physics, 2002, 35(24)：5141-5151.

[26] YOSHIKAWA Y, UMEKI T, MUKAE T, et al. Frequency stabilization of a laser diode with use of light-induced birefringence in an atomic vapor[J]. Applied optics, 2003, 42(33)：6645-6649.

[27] ČÍP O, PETRŮ F, MATOUŠEK V, et al. Direct measurement of index of refraction of air by means of high-resolution laser interferometry[J]. Physica scripta, 2005, T118：48-50.

[28] BIRCH K, DOWNS M. An updated Edlén equation for the refractive index of air[J]. Metrologia, 1993, 30(3)：155-162.